Thin-core fiber-optic biosensor for DNA hybridization detection*

LONG Shao-cong (龙少聪)**, ZHU Yan-ru** (朱彦儒)**, HU Mu-yun** (胡慕芸)**, QI Yi-fan** (祁一凡)**, JIANG Yun-rui** (蒋韵睿)**, LIU Bo** (刘波)****, and ZHANG Xu** (张旭)

Tianjin Key Laboratory of Optoelectronic Sensor and Sensing Network Technology, Institute of Modern Optics, Nankai University, Tianjin 300350, China

(Received 10 April 2018; Revised 29 May 2018)

A real-time label-free DNA biosensor based on thin-core fiber (TCF) interferometer is demonstrated experimentally. The proposed biosensor is constructed by splicing a TCF between two segments of single mode fibers (SMFs) and integrated into a microfluidic channel. By modifying the TCF surface with monolayer poly-l-lysine (PLL) and single-stranded deoxyribonucleic acid (ssDNA) probes, the target DNA molecules can be captured in the microfluidic channel. The transmission spectra of the biosensor are measured and theoretically analyzed under different biosensing reaction processes. The results show that the wavelength has a blue-shift with the process of the DNA hybridization. Due to the advantages of low cost, simple operation as well as good detection effect on DNA molecules hybridization, the proposed biosensor has great application prospects in the fields of gene sequencing, medical diagnosis, cancer detection and environmental engineering.

Document code: A **Article ID:** 1673-1905(2018)05-0346-4

DOI https://doi.org/10.1007/s11801-018-8054-5

The technology of deoxyribonucleic acid (DNA) detection plays an irreplaceable role in many fields, such as genetic research, medical diagnosis, drug examination, environmental engineering and bioengineering[1-3], which makes great contributions to human health, environmental protection and scientific development. Traditional DNA detection method based on fluorescence has accessed rapid development[4]. In recent years, the research of biosensor based on fiber-optic sensing technology has attracted wide attention. The fiber-optic biosensors have many advantages, such as miniaturization, flexible structure, fast response, low cost and label-free. They also have high sensitivity and can react in a very short period of time, which is very suitable in the biological detection areas. Therefore, the fiber-optic biosensors have been widely used in the field of biomolecules detection, including DNA, protein, bacteria and viruses, etc.

In the past few years, various fiber-optic structures with different mechanisms have been designed and proposed for biological detection, including evanescent field effect[5], surface plasmon resonance (SPR) effect[6,7], whispering gallery mode resonator and modal interference effect[8]. They all show precious biological sensing properties as well as potential application value. The evanescent fiber biosensors have the advantages of anti-electromagnetic interference and high transmission bandwidth[9]. The fiber SPR technique further increases the detection sensitivity and has drawn much attention in the field of biosensing[10]. However, the SPR performance depends on the metal coating thickness, and noble metals with good biocompatibility, such as gold and silver, are expensive. Thus, the SPR fiber sensor is difficult to fabricate and hard to meet the practical needs. Whispering gallery mode resonator has low detection limit, while it also needs a flexible system.

Due to the advantages of small volume, high sensitivity, label-free and ease of fabrication, fiber-optic modal interference devices are investigated, such as Michelson interferometer[11], Sagnac interferometers[12] and Mach-Zehnder (M-Z) interferometers[13]. The constraint capability of guided-mode light in the thin-core fiber (TCF) is much weaker than that in conventional SMF, and the mode field diameter of the TCF is larger than that of standard SMF. Thus, more high-order modes will be excited to form modal interference. Fiber-optic sensors based on modal interference in the TCF possess excellent properties, which makes them applicable for the measurement of different physical parameters. For example, Deng et al[14] have utilized TCF based sensor to achieve the determinations of hydrogen sulfide gas. Ruan

* This work has been supported by the National Undergraduate Innovation Training Program (No.201710055065).

** E-mail: liubo@nankai.edu.cn

et al[15] have adopted TCF structure to achieve temperature measurement. These TCF-based sensors which exhibit outstanding sensing performances showing the modal interference effect in the TCFs could be exploited for external response detection. Therefore, the combination of TCFs system provides a promising approach for biomedical field.

In this paper, a TCF based fiber-optic modal interferometer is proposed for the detection of DNA hybridization. Hydrofluoric acid (HF) is employed to corrode the TCF to reduce the diameter of the TCF, thus the evanescent field effect can be enhanced and the sensitivity of the proposed sensor can be improved. A microfluidic channel integrated with the TCF structure is designed for the lead-in and lead-out of the bio-samples. The hybridization response between the probe DNA and the target DNA on the fiber surface is detected by tracing the shift of the resonance wavelength occurring in the transmission spectra. With the advantages of low cost, ease of operation, fast response to DNA hybridization, the proposed fiber sensor has great potential value in genetic research, medical diagnosis, cancer screening and environmental engineering.

Schematic diagram of the TCF based fiber sensor is shown in Fig.1. In the SMF-TCF-SMF based fiber structure, the incident light is coupled from the input SMF into the TCF, and then a series of linear polarization modes can be excited due to the modal field mismatch. After the core mode and cladding modes propagate in the TCF, modal interference will occur. According to modal interference, the phase different Φ between the core mode and the jth cladding mode can be approximated as $\Phi=2\pi\Delta n_{\text{eff}}L/\lambda$, where Δn_{eff} is the effective refractive index difference of the core mode and jth cladding mode. If $\Phi=(2K+1)\pi$, the interference wavelength dip positions λ_{D} can be obtained by [16]

$$2\pi[n_{\text{eff}}^{\text{co}}(\lambda) - n_{\text{eff}}^{\text{cl},j}(\lambda, n_{\text{ext}})]\frac{L}{\lambda_{\text{D}}} = (2K+1)\pi, \quad (1)$$

where $n_{\text{eff}}^{\text{co}}$ is the effective refractive index of the core mode, $n_{\text{eff}}^{\text{cl},j}$ is the effective refractive index of the jth order cladding mode, n_{ext} is the external refractive index, L is the length of the inserted TCF, and K is an integer.

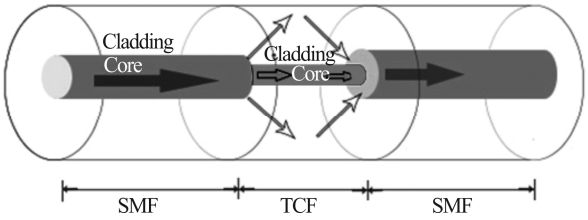

Fig.1 Schematic diagram of the TCF based fiber sensor

According to Eq.(1), the relation between the corresponding wavelength and the external refractive index variation can be described as[17]

$$\frac{d\lambda_{\text{D}}}{dn_{\text{ext}}} = \frac{-\lambda_{\text{D}}}{\Delta n_{\text{eff}}}\frac{\partial n_{\text{eff}}^{\text{cl},j}}{\partial n_{\text{ext}}} / [1 - \frac{\lambda_{\text{D}}}{\Delta n_{\text{eff}}}(\frac{\partial n_{\text{eff}}^{\text{co}}}{\partial \lambda} - \frac{\partial n_{\text{eff}}^{\text{cl},j}}{\partial \lambda})]. \quad (2)$$

When the external refractive index changes, the corresponding cladding mode will be changed, and the corresponding phase matching condition also can be changed, resulting in the observable shift of the transmission spectrum.

The biomaterials used in our experiment include poly-l-lysine (PLL) (sigma, molecular weight: 30 000—70 000, 0.1 mg/mL), PBS buffer (0.01 mmol Na_2HPO_4, 0.15 mol NaCl, pH=7.4), TE buffer (10 mmol Tris-HCl, 1 mmol EDTA, pH=7.4), probe DNA (Genewiz, 1 pmol/μL) and target DNA (Genewiz, 0.5 pmol/μL).

The PLL/PBS solution is prepared in PLL and PBS buffer. The probe DNA and target DNA solution is dissolved in TE buffer, respectively. The corresponding DNA sequences of the probe DNA and target DNA are as shown in Tab.1.

Tab.1 DNA sequences of probe DNA and target DNA

Name	DNA sequence
Probe DNA	5'-CAG CGA GGT GAA AAC GAC AAA AGG G-3'
Target DNA	5'-CC CTT TTG TCG TTT TCA CCT CGC TG-3'

The experimental setup of the DNA detection system is shown in Fig.2. The TCF (Nufern, 460-HP) used in the experiment possesses the length of 50 mm and core diameter of 3.0 μm. The TCF is spliced between two sections of conventional SMFs (SMF-28e) by using a commercial fusion splicer (FITEL, ver.2). The TCF section is corroded in HF for 50 min, and then the remaining cladding diameter of the corroded TCF is about 62.805 μm, as shown in Fig 3.

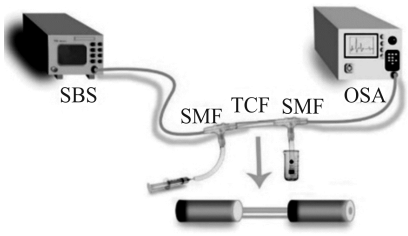

Fig.2 Schematic diagram of experimental setup for DNA hybridization detection system

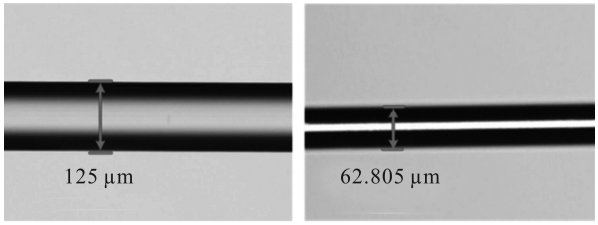

Fig.3 Side view micrographs of the TCF before and after HF corrosion

Then the fabricated sensing structure is inserted into a micro-flow channel encapsulating with tube and T-branch pipe. All of the liquid samples are injected into the microchannel by using a syringe pump. Light from a supercontinuum broadband source (SBS) is launched into the TCF modal interferometer, and the interferometric transmission spectrum is monitored by employing an optical spectrum analyzer (OSA, Yokogawa AQ6370C) with operation wavelength ranging from 600 nm to 1 700 nm and a wavelength resolution of 0.2 nm. It should be noted that the diameter and the length of TCF have an influence on the mode distribution and the modal interference, respectively. To investigate light propagation in the TCFs with different cladding diameters, a three-dimensional simulation is utilized to analyze the light beam characteristics by the beam propagation method. Figs.4(a) and (b) show that the simulated amplitude distribution of the light propagating in the TCF with the cladding diameters of 125 μm and 62.805μm, respectively. In the simulation process, the TCF has a core diameter of 3.0 μm and a length of 50 mm. The refractive indexes of cladding and core are 1.444 7 and 1.450 4 at 1 550 nm, respectively. It indicates that the distribution of the modes field is more strongly affected by the different cladding diameters of the TCF section. It also presents a stronger coupling with the fiber cladding modes in the corroded TCF. Thus, the propagating light becomes more sensitive to the variation of external medium.

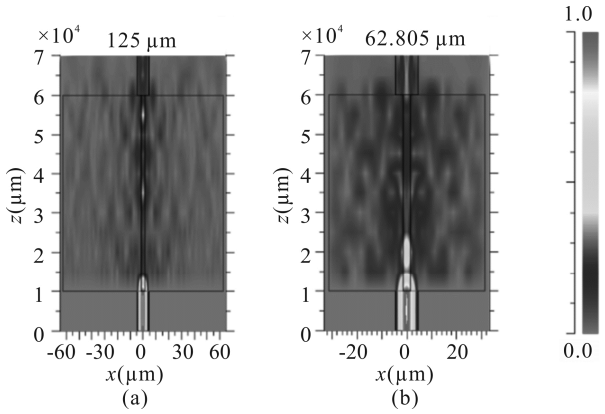

Fig.4 Simulation of beam propagation process with the cladding diameters of (a) 125 μm and (b) 62.805 μm, respectively

Steps for the detection of DNA hybridization are as follow.

(1) Pump the PLL solution into the micro-flow channel to achieve surface function of TCF for 60 min, followed by rinsing with distilled water for 5 min.

(2) After the TCF surface is functionalized and excess PLL is wiped off, the probe DNA solution is pumped into the channel for 1 h. The PLL amidogen groups on the TCF surface are achieved to attach the probe DNA molecules. After sufficient reaction between PLL and probe DNA molecules, deionized water is injected into the microfluidic channel to remove any non-reacted probe DNA.

(3) Injecting the complete complementary target DNA solution into the microfluidic channel, and transmission spectral responses of the DNA hybridization process are monitored in real time.

Fig.5 shows the schematic diagram of the DNA hybridization procedure. During the experimental process, PLL is adsorbed on the surface of the TCF through electrostatic action. When the probe DNA molecules are gradually added, the probe DNA will bind to the PLL. The target DNA binding with the probe DNA molecules can change the refractive index near the fiber surface by the base complementary pairing, which leads to the wavelength shift in the transmission spectrum.

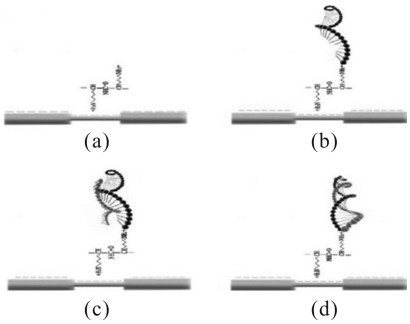

Fig.5 Schematic diagram of the DNA hybridization procedure: (a) surface functionalization of the TCF; (b) immobilization of probe DNA; (c) and (d) dynamic process for the binding of target DNA with immobilized probe DNA in the microchannel

Fig.6 shows that the transmission spectrum of the TCF modal interferometer corresponds with those of the PLL, the probe DNA and the target DNA while the reaction is going. And the transmission spectrum comes to stabilization eventually. Adding PLL, probe DNA and target DNA step by step, the steady trough positions of the system are 1 468.0 nm, 1 467.4 nm and 1 467.2 nm, with the corresponding losses of −20.506 19 dB, −20.360 04 dB and −20.188 54 dB, respectively. After adding all the substances, we can observe the wavelength blue shift as well as the increase of light intensity. They are all gradually stabilized with the increase of time. The experimental results show that the wavelength and the intensity of the resonance dips change while the probe DNA and the target DNA are added. It is reliable as the biosensor is used to detect the variation of wavelength and intensity during DNA hybridization, which means that the sensor is reliable when it comes to detect the wavelength and intensity change during DNA hybridization.

Injecting PLL, probe DNA and target DNA molecules which have larger refractive index than optical fiber in the microfluidic channel affects the effective refractive index of the propagating cladding modes, leading to the wavelength shift. It can be seen that when the effective

refractive index of the cladding modes increases, the resonant peak will have blue-shift.

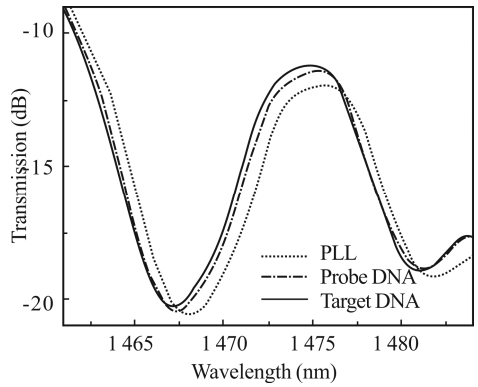

Fig.6 Transmission spectra of the TCF based sensor at different experimental processes

Fig.7 shows the relative wavelength shift responses of the detection system to TCF surface functionalization and DNA hybridization processes. The results indicate that when the probe DNA and target DNA happen to hybridization, the wavelength shift is about 0.2 nm, which achieves the identification detection of DNA hybridization processes.

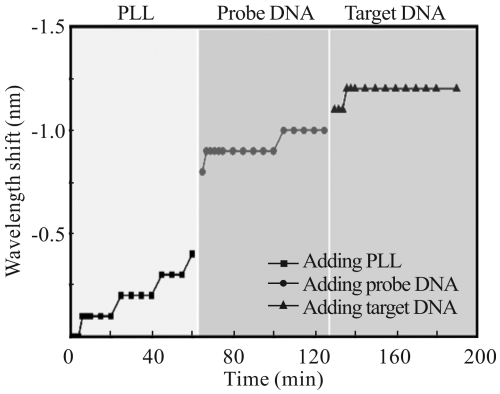

Fig.7 The real-time relative wavelength shift responses to fiber surface functionalization and DNA hybridization processes

In conclusion, a biosensor for DNA hybridization detection based on TCF is demonstrated. The transmission spectral characteristics of the TCF-based biosensor are experimentally as well as theoretically investigated to evaluate the DNA hybridization detection. Experimental results indicate that the label-free detection of double stranded DNA hybridization can be realized by utilizing the microchannel. The fiber-optic microfluidic channel based on the integration of the TCF has the advantages of simple structure, low production cost and rapid response. It has great application prospects in medical diagnosis, cancer detection, environmental engineering and other fields.

References

[1] Kleinjung F, Bier F F, Warsinke A and Frieder W Scheller, Analytica Chimica Acta **350**, 51 (1997).

[2] Schmidt PM, Lehmann C, Matthes E and Bier FF, Biosensors & Bioelectronics **17**, 1081 (2002).

[3] Candiani A, Bertucci A, Giannetti S, Konstantaki M, Manicardi A, Pissadakis S, Cucinotta A, Corradini R and Selleri S, Journal of Biomedical Optics **18**, 057004 (2013).

[4] Long F, Wu S, He M, Tong T and Shi H, Biosens & Bioelectron **26**, 2390 (2011).

[5] Shitong Han, Xiaohong Zhou, Yunfei Tang, MiaoHe, Xinyu Zhang, Hanchang Shi and Yu Xiang, Biosensors & Bioelectronics **6**, 265 (2016).

[6] Kant R, Tabassum R and Gupta B D, Biosensors & Bioelectronics **99**, 637 (2018).

[7] Ding ZW, Lang TT, Wang Y and Zhao CL, Journal of Lightwave Technology **35**, 4734 (2017).

[8] Song BB, Zhang H, Liu B, Lin W and Wu J, Biosensors & Bioelectronics **81**, 151 (2017).

[9] Chandra S, Bharadwaj R and Mukherji S, Sensors and Actuators B Chemical **240**, 443 (2017).

[10] YC Tan, WB Ji, V. Mamidala, K.K. Chow and S.C. Tjin, Sensors and Actuators B **196**, 260 (2014).

[11] G. Salceda-Delgado, A. Martinez-Rios, R. Selvas-Aguilar, R. I. Álvarez-Tamayo, A. Castillo-Guzman, B. Ibarra-Escamilla, V. M. Durán-Ramírez and L. F. Enriquez-Gomez, Sensors **17**, 1259 (2017).

[12] Shiying Xiao, Yue Wu, Yue Dong, Han Xiao, Youchao Jiang, Wenxing Jin, Haisu Li and Shuisheng Jian, Optics & Laser Technology **96**, 254 (2017).

[13] Xianfeng Chen, Lin Zhang, Kaiming Zhou, Edward Davies, Kate Sugden, Ian Bennion, Marcus Hughes and Anna Hine, Optics Letters **32**, 2541 (2007).

[14] Dashen Deng, Wenlin Feng, Jianwei Wei, Xiang Qin and RongChen, Applied Surface Science **423**, 492 (2017).

[15] Ruan J, Hu LR, Lu AS and Xu HG, IEEE Photonics Technology Letters **29**, 1364 (2017).

[16] Meng J, Ze MW, Zhong ZZ and Zhang YX, Microwave & Optical Technology Letters **59**, 53 (2017).

[17] Bao, Weijia, Hu Naifei, Qiao Xueguang, Rong Qiangzhou, Wang Ruohui, Yang Hangzhou, Yang Tingting and Sun An, IEEE Photonics Technology Letters **28**, 2245 (2016).